MDPI

Article

Annual and Seasonal Precipitation and Their Extremes over the Tibetan Plateau and Its Surroundings in 1963–2015

Jin Ding [1] , **Lan Cuo** [2,3,4,5,]*, **Yongxin Zhang** [6], **Cunjie Zhang** [7], **Liqiao Liang** [2,3] **and Zhe Liu** [2,3]

1   Public Meteorological Service Center, China Meteorological Administration, Beijing 100081, China; djforpub@163.com
2   Key Laboratory of Tibetan Environment Changes and Land Surface Processes, Institute of Tibetan Plateau Research, Chinese Academy of Sciences, Beijing 100101, China; liangliqiao@itpcas.ac.cn (L.L.); liuzhe@itpcas.ac.cn (Z.L.)
3   University of Chinese Academy of Sciences, Beijing 100864, China
4   Center for Excellence in Tibetan Plateau Earth Sciences, Beijing 100101, China
5   ECMI Team, State Key Laboratory of Tibetan Plateau Earth System Science, Institute of Tibetan Plateau Research, Chinese Academy of Sciences, Beijing 100101, China
6   Research Applications Laboratory, National Center for Atmospheric Research, Boulder, CO 80305, USA; zhangyx@ucar.edu
7   National Climate Center, China Meteorological Administration, Beijing 100081, China; zhangcj@cma.gov.cn
*   Correspondence: lancuo@itpcas.ac.cn

Abstract: Based on daily precipitation data from 115 climate stations, seasonal and annual precipitation and their extremes over the Tibetan Plateau and its surroundings (TPS) in 1963–2015 are investigated. There exists a clear southeast-northwest gradient in precipitation and extreme daily precipitation but an opposite pattern for the consecutive dry days (CDDs). The wet southeast is trending dry while the dry center and northwest are trending wet in 1963–2015. Correspondingly, there is a drying tendency over the wet basins in the southeast and a wetting tendency over the dry and semi-dry basins in the center and northwest in summer, which will affect the water resources in the corresponding areas. The increase (decrease) in precipitation tends to correspond to the increase (decrease) in maximum daily precipitation but the decrease (increase) in CDDs. Extreme precipitation events with 20-year, 50-year, 100-year, and 200-year recurrence occurred frequently in the past decades especially in the 1980s. The greatest extreme precipitation events tend to occur after the late 1990s and in the southeastern TPS. The ERA5 reanalysis and climate system indices reveal that (1) decreased moisture transports to the southeast in summer due to the weakening of the summer monsoons and the East Asian westerly jet; (2) increased moisture transports to the center in winter due to the strengthening of the winter westerly jet and north Atlantic oscillation; and (3) decreased instability over the southeast thus suppressing precipitation and increased instability over the northwest thus promoting precipitation. All these are conducive to the drying trends in the southeast and the wetting trends in the center.

Keywords: Tibetan Plateau; mean and extreme precipitation; precipitation trends; recurrence of extreme precipitation events; atmospheric circulation indices

1. Introduction

Climate change over the Tibetan Plateau (TP) and its surroundings (TPS) in the recent decades has received much attention [1–8] due to (a) the TPS being the headwater of several major Asia Rivers, (b) the TPS exerting significant influence on the regional and global climate owing to its massive size and high elevation, and (c) climate change on the TPS having important impacts on the social and economic aspects of the region and its surrounding areas. Among all of the examined variables, precipitation is especially emphasized due to its direct impacts on water resources, the environment, glaciers, and ecosystems [9,10]. A good understanding of precipitation characteristics and its changes

over the TP have been gained. However, many of these studies suffer from shortcomings including (a) relatively shorter data records for examining trends and extremes, (b) not considering the entire TPS, (c) focusing on the limited number of individual river basins, and (d) lacking analyses in relation to climate systems and physical mechanisms behind the changes. This study aims to fill the gaps.

The TPS features complex topography and is characterized by diverse climate and ecosystems. Mean annual precipitation ranges widely from ~20 mm in the northwest to ~1900 mm in the southeast. Wet season (May–September) precipitation not only accounts for more than 70% of the annual total, but also displays distinctive vertical gradients that vary with elevation and sub-regions in the TPS [11]. In contrast to the prevailingly warming trends in the recent decades over the TPS [12], changes in precipitation do not show consistent and uniform plateau-wide trends both temporally and spatially. For example, Lin and Zhao [13] reported that in the central and northeast TP precipitation decreased by 10–40 mm·decade^{-1} from 1950s to early 1990s, while in the interior, precipitation changes varied with time and sub-regions. Cuo et al. [3] showed that the northwest (northeast) of the northern TP became dryer (wetter) in 1957–2009, and the south of the northern TP experienced insignificant changes. Such heterogeneous changes likely resulted from the complex interplay among the terrain, local and large-scale climate systems, and atmospheric teleconnections. Thus, studies focusing on the sub-regions may not fully reveal the overall precipitation patterns and the associated climatic conditions over the vast TPS.

Likewise, changes in precipitation extremes on the TP vary depending on the time periods, sub-regions, and atmospheric circulation indices examined. For example, You et al. [14] reported non-significant increase trends for heavy precipitation days, maximum 1-day precipitation, and total precipitation on extreme wet days but decrease trends for maximum 5-day precipitation, consecutive wet and dry days during 1961–2005 in the eastern and central TP. Ge et al. [15] noted heterogeneous change patterns in 10 extreme precipitation indices defined by the Expert Team on Climate Change Detection and Indices (ETCCDI) for 1975–2014 at 83 stations on the TP, and showed a significant increase trend in the proportion of extreme precipitation to the annual total. This work extends the analysis periods to the entire TPS and also examines seasonal changes, in addition to annual changes.

As the "Water Tower" of Asia, the TPS is home to several large and trans-boundary rivers that provide water resources for 1.65 billion people and numerous ecosystems locally and downstream. There are also internal rivers and basins on the TPS, such as the Chaidamu Basin and Qinghai Lake basin (CQB), Changtang basin (CTB), and northern Qilian Mountain basins (NQMB) that support the local societies and ecosystems. Clearly, understanding basin-wide precipitation changes is important for water resources management as these rivers are essentially fed by precipitation [4]. Quite a few studies have examined precipitation changes in many individual basins on the TPS; however, direct comparisons among the basins are difficult due to differences in the time periods or contradictory findings among the published studies. For example, Wang Y. et al. [16] documented non-significant precipitation declines in the Yangtze River basin (YTR) by 0.40 mm·year^{-1} during 1960s–2000s, while Tian et al. [17] reported little change in the spatially averaged annual and seasonal mean precipitation for YTR and the Yellow River basin (YLR) during 1957–2013. Jiang et al. [18], on the other hand, showed precipitation decreases by 0.27 mm·year^{-1} in autumn but increases in the other seasons and annual totals for YLR during 1956–2012.

For the Mekong River basin (MKR), one of the trans-boundary river systems and for which more than 80% precipitation occurs during summer and autumn, Wu et al. [19] noted significantly increasing precipitation in spring but only slight increase for annual totals in 1960–2009. Over the Salween River basin (SWR), another trans-boundary river system, Yang et al. [20] showed increases in maximum daily precipitation at most stations but varying trends in the frequency and intensity of annual extreme precipitation during

1971–2010. For the endorheic Tarim River basin (TRB), Deng and Chen [21] reported an increasing trend of 0–3 mm·year^{-1} in annual precipitation during 2000–2013. Precipitation increase was also documented for the Qinghai Lake basin during 2000–2012, which resulted in the expansion of the lake [22]. As a reference, the mean annual precipitation is below 150 mm for TRB and below 100 mm for the Chaidamu basin, both located in the desert area, and is 224.9 mm for CTB [23].

The generation of precipitation requires moisture, lifting, and condensation. Lifting can be provided by weather systems such as low-pressure systems or topography, while condensation is the process by which water vapor in the air is changed into liquid water, both of which are related to the stability of the atmosphere. A stable atmosphere resists the vertical movement of air parcels leading to little or no precipitation but in an unstable atmosphere, the air parcel could rise and cloud droplets form when the air parcel reaches the condensation level, leading to precipitation. Thus, changes in moisture and stability will lead to changes in precipitation characteristics. For example, Cuo and Zhang [11] and Sun et al. [24] examined water vapor and stability of the atmosphere over the TP and satisfactorily explained the development of the vertical gradients of precipitation in the region. However, examination of the spatiotemporal patterns of water vapor and stability of the atmosphere over the TPS and their connection to precipitation trends is limited and this is one area that this work will also explore.

The objective of this study is two-fold: (1) Examining the means and changes of seasonal and annual precipitation and their extremes over the entire TPS and the river basins, and (2) investigating the possible connections between the atmosphere circulation systems and precipitation as well as between water vapor/atmospheric stability and precipitation with the aim of explaining the reasons behind the changes of precipitation. It is hoped that this study will provide valuable information for climate change status and water resources management on the TPS.

2. Methods

2.1. Study Domain

The TPS (26–40° N, 78–106° E) is the highest land mass in the world with an average elevation of about 4000 m and an area of approximately 2.5×10^6 km^2. It consists primarily of the Tibetan Autonomous Region (referred to as T hereafter) and Qinghai Province (Q), but also includes the southern Xinjiang Uygur Autonomous Region (X), part of Gansu Province (G), western Sichuan Province (S), and northern Yunnan Province (Y) (Figure 1). The TPS is surrounded by the Himalayas in the south, the Tianshan in the northwest, the Karakoram and the West Kunlun in the west, the Qilian Mountain in the north, and the Hengduan Mountains in the southeast. The East Kunlun, the Bayankela, the Tanggula, the Nianqing-tanggula, and the Gangdise Mountains rolling from the west to the east are located in the interior TPS dividing the TPS into headwaters of 13 large river, including YLR and YTR in the east, MKR, SWR, and Irrawady in the southeast, Brahmaputra basin (BPR) and Ganges in the south, Indus River basin (IDR) in the southwest, Amu Darya and Syr Darya in the west, Ili River and China's largest endorheic TRB in the northwest, and NQMB in the northern flank of the Qilian Mountain. There are also some smaller endorheic basins, such as CQB in the north and CTB in the west (Figure 1).

2.2. Data

Observed daily precipitation is obtained from the website of Climate Data Center of China Meteorological Administration in Beijing, China (CMA; data.cma.cn, last accessed on 11 May 2021). The quality of the station data is thoroughly controlled through two steps: Removing any abnormal values such as negative and unreasonably large values, and identifying missing values and filling in the gaps by interpolation (see Ding et al. [12] for details). After the quality control, precipitation observations at 115 stations in 1963–2015 are selected for analyses. The length of the daily time series ranges from 22 to 31 days in any given month, sufficient for representing monthly precipitation conditions. The

selected weather stations are shown in Figure 1 and their details are listed in Table S1 of the Supplementary Material.
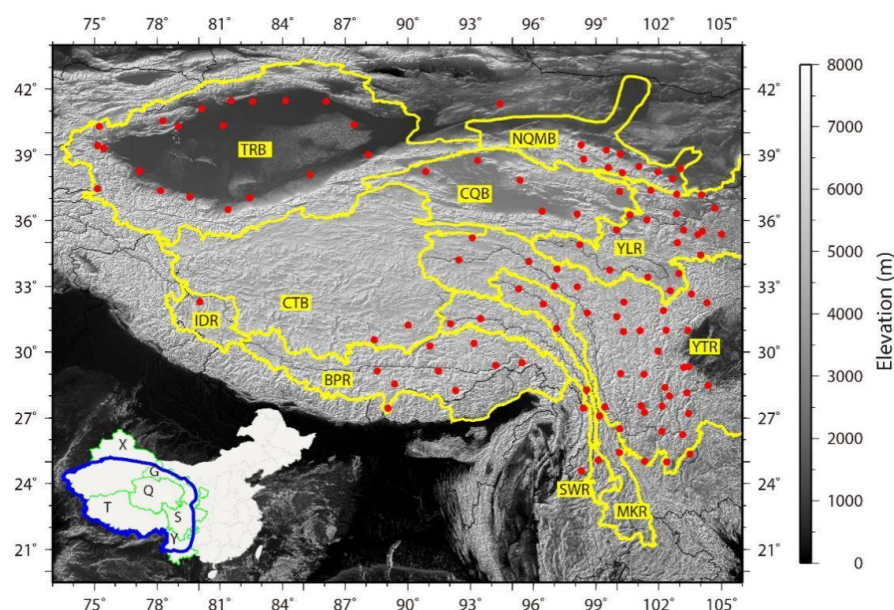

Figure 1. The geographic locations of the study area and the weather stations on the Tibetan Plateau and the surroundings (TPS) used in the study. The blue line in the inset represents the study area and green lines represent the boundaries of the 6 provinces including the Tibet Autonomous Region (T), Qinghai Province (Q), Xinjiang Uygur Autonomous Region (X), Gansu Province (G), Sichuan Province (S), and Yunnan Province (Y). Red points denote the weather stations. Yellow lines represent the boundaries of the ten basins on the TPS: The Yellow River basin (YLR), the Yangtze River basin (YTR), the Mekong River basin (MKR), the Salween River basin (SWR), the Brahmaputra river basin (BPR), the Indus River basin (IDR), the Tarim River basin (TRB), the Northern Qilian Mountain river basin (NQMB), the Changtang Basin (CTB), and the Chaidamu and Qinghai Lake basins (CQB) in the interior TPS.

Derived precipitation variables based on daily precipitation during 1963–2015 at each station include total precipitation, maximum precipitation, and maximum length of dry spell at seasonal and yearly time scales. Seasonal precipitation is the total precipitation in a season (winter: December–February, spring: March–May, summer: June–August, autumn: September–November). Seasonal maximum precipitation is the maximum value of daily precipitation in a season. The maximum length of dry spell is the maximum number of consecutive dry days (CDD) with daily precipitation < 1.00 mm. Annual values are calculated in the same way, except that the time span is yearly.

For river basins, the derived precipitation variables are obtained by averaging the corresponding quantities over the stations that fall in each basin. Depending on the quality and availability of the data, the numbers of stations in the basins vary widely from one for IDR to thirty-seven for YTR (Figure 1, Table 1, Table S1).

Regional climate is affected not only by large-scale circulations in the region and their interactions with local terrain, but also by teleconnections of climate systems. Over the TPS, there are several circulation and teleconnection patterns that have been identified to directly or indirectly affect the climate including the Indian summer monsoon (ISM), Western North Pacific monsoon (WNPM), East Asian Westerly Jet (WJ), El Niño and Southern Oscillation (ENSO), Tibetan Plateau High (TH), and North Atlantic Oscillation (NAO). These circulations and climate systems represented by their indices have been examined in the context of precipitation spatiotemporal distributions in the TPS mainly for specific sub-regions [3,25–33]. In this work, we extend the analysis to the entire TPS using all six indices. Table 2 lists the definitions and sources of these indices.

Table 1. Seasonal and annual precipitation (mm) and trends (mm·y^{-1}) over the ten river basins during 1963–2015. Bold fonts represent statistically significant trends ($p < 0.05$). Numbers in brackets denote the numbers of weather stations that are located in each of the basins.

	BPR(9)	CQB(6)	CTB(2)	IDR(1)	MKR(5)	NQMB(10)	SWR(4)	TRB(20)	YLR(18)	YTR(37)
	Seasonal and annual precipitation									
spring	96.6	22.8	25.0	5.0	119.4	34.3	111.5	20.9	119.4	133.8
summer	316.4	84.7	225.3	53.3	390.3	130.7	360.6	44.2	279.3	463.7
autumn	106.3	20.5	60.6	8.2	160.4	40.2	157.8	13.4	122.9	185.1
winter	11.5	4.2	4.1	4.1	34.9	4.7	25.1	5.8	20.4	21.2
annual	530.8	131.9	315.2	70.6	708.2	209.8	658.3	84.3	543.6	803.2
	Trends of seasonal and annual precipitation									
spring	**0.2167**	0.0087	**0.1280**	−0.0047	**0.1194**	0.0233	0.1937	0.0112	0.0627	0.1065
summer	−0.0407	0.1281	0.1614	−0.0522	−0.1753	0.1226	−0.1416	0.0835	−0.0927	−0.1534
autumn	0.0791	0.0092	0.0574	−0.0024	0.1273	0.0487	0.0643	0.0254	0.0015	−0.0909
winter	0.0154	0.0013	0.0084	−0.0015	−0.0115	0.0041	−0.0298	0.0009	−0.0041	−0.0131
annual	0.9860	0.3610	1.9022	−0.0200	−0.1686	0.6970	0.4503	0.5420	−0.1273	−0.4120

Table 2. Selected climate system indices.

Climate System Index	Abbreviation	Definition/Reference	Data Source	Available for Months
Indian Summer Monsoon Index	ISM	Wang and Fan [34], Wang et al. [35]	Asia-Pacific Data-Research Center (APDRC; http://apdrc.soest.hawaii.edu/projects/monsoon/seasonal-monidx.html, last accessed on 12 May 2021)	6–9
Western North Pacific Monsoon Index	WNPM	Wang and Fan [34], Wang et al. [35]	Asia-Pacific Data-Research Center (APDRC; http://apdrc.soest.hawaii.edu/projects/monsoon/seasonal-monidx.html, last accessed on 12 May 2021)	6–9
East Asian Westerly Jet Index	WJ	Duan and Wu [36]	Duan and Wu (2009)	1–12
ENSO	ENSO	Multivariate El Niño/Southern Oscillation (ENSO) index is the time series of the leading combined EOF of 5 different variables over the tropical Pacific basin, 30 S–30° N, 100 E–70° W	National Oceanic and Atmospheric Administration (NOAA; https://www.esrl.noaa.gov/psd/enso/mei/, last accessed on 12 May 2021)	1–12
North Atlantic Oscillation	NAO	NAO index is based on the surface sea-level pressure difference between the Subtropical (Azores) High and the Subpolar Low	National Oceanic and Atmospheric Administration (NOAA; https://www.ncdc.noaa.gov/teleconnections/nao/, last accessed on 12 May 2021)	1–12
Tibet Plateau High Index	TH	At 500 hPa pressure level, the accumulated value of cell area multiplied by the difference between cell geopotential height (GPM) and 5000 GPM in 30 N–40° N, 75 E–105° E	China Meteorological Administration (CMA)	1–12

The atmospheric conditions including water vapor and stability will be examined using the ERA5 reanalysis at 0.25° resolution from the European Center for Medium-range Weather Forecasts [37]. ERA5 uses the most recent Earth system modeling and data assimilation techniques and assimilates vast amounts of historical observations. ERA5 has been shown to exhibit consistent improvement over the widely used ERA-Interim reanalysis [38] in land surface variables and atmospheric variables [39].

2.3. Methods

2.3.1. Trend Test

The Mann—Kendall test [40,41] is a non-parametric test, and has been used extensively in hydrological and meteorological research [3,42–44]. The non-parametric Sen's slope [45] is used to quantify the monotonic trends of precipitation variables during 1963–2015. The details of the trend test are described in Ding et al. [12].

2.3.2. Gumbel Distribution

Gumbel distribution [46] has been widely used in hydrological frequency analyses, such as precipitation and snowmelt flood or precipitation extremes [47–49]. Gumbel distribution function of a threshold is defined as:

$$F(x) = e^{-e^{-a(x-u)}} \tag{1}$$

where $a = \frac{S_y}{S_x}$ and $u = E_X - \frac{S_x}{S_y}E_y$ are the main parameters determined by the expected values (Ex and Ey) and mean square deviations (s_x and s_y) calculated in Equations (2)–(5) below for series $x_s = (x_1, x_2, ..., x_n)$ (x_i is the *i*th x value for a sample of size n). Here, $y_i = -ln(-ln\frac{i}{n+1})$, the *i*th y value for a sample of size n.

$$E_x = \frac{1}{n} \sum_{i=1}^{n} x_i \tag{2}$$

$$E_y = \frac{1}{n} \sum_{i=1}^{n} y_i \tag{3}$$

$$S_x = \sqrt{\frac{1}{n} \sum_{i=1}^{n} (x_i - E_x)^2} \tag{4}$$

$$S_y = \sqrt{\frac{1}{n} \sum_{i=1}^{n} (y_i - E_y)^2} \tag{5}$$

The threshold (x_p) for a specified recurrence period can be constructed through probability analysis using the following formula:

$$x_p = u - \frac{1}{a}ln[-ln(1-P)] \tag{6}$$

where P is probability or the reciprocal of recurrence period. In our study, 20, 50, 100, and 200 years are selected as the recurrence periods and our focus is on the maximum daily precipitation series at a yearly time scale.

2.3.3. Goodness of Fit Test for Recurrence Period

Chi-square (χ^2) test is often used to test the distinctions between two or more samples [7,50]. The statistical formula for Chi-square (χ^2) test is the following:

$$x^2 = \sum_{i=1}^{k} \frac{(OF - ER)^2}{EF} \tag{7}$$

where *EF* is the expected cell frequency (the frequency corresponding to the recurrence period), *OF* is the observed cell frequency (the proportion of actual occurrences in the sample size), and k is the total number of time series. According to the Chi-square test critical table, when $\alpha = 0.05$, the critical value is 69.832.

2.3.4. Maximum Length of Dry Spell—CDD

CDD is one of the 27 indices of climate extremes as defined by the ETCCDI (http://etccdi.pacificclimate.org/list_27_indices.shtml, last accessed on 12 May 2021). CDD is commonly used in the assessment of drought persistence and extremes [51–55]. From the time series of consecutive days in a month, the longest consecutive days with daily precipitation < 1 mm are selected as seasonal CDD. For annual CDD, precipitation in the wet season (May–September) is used for practically representing the drought conditions in the region since the wet season precipitation accounts for more than 70% of the annual totals in the TPS [11,56].

3. Results

3.1. Temporal and Spatial Distributions of Precipitation

Seasonal mean precipitation (unit: mm) during 1963–2015 ranges from 0.6 at Rikaze in T in winter to 998.0 at Emeishan in S in summer (Figure 2). There is a clear southeast-northwest precipitation gradient on the TPS in summer and to a lesser extent in autumn and spring. The southern X, western T, northern Q, and northern G are dry throughout the year. The spatiotemporal distributions of seasonal maximum daily precipitation (Figure 2) are quite similar to those of seasonal precipitation, i.e., gradually decreasing from the southeast to the northwest, and low in winter but large in summer (also largest at Emeishan and lowest at Rikaze). The stations that record higher maximum daily precipitation generally correspond to higher seasonal precipitation as well, suggesting that extreme precipitation events may have contributed substantially to the seasonal totals at the stations. Seasonal mean CDDs during 1963–2015 (unit: days) range from 4.6 at Tengchong in Y in summer to 88.0 at Rikaze in T in winter and gradually increase from the southeast to the northwest (Figure 2), opposite to what seasonal mean precipitation shows spatially. Stations in the west such as Lenghu in Q, Jiangzi and Shiquanhe in T, Qiemo, Tieganlike, Hetian, and Ruoqiang in X tend to experience persistent drought throughout the year.

Annual precipitation (unit: mm) decreases from the southeast to the northwest (Figure 3a), similar in spatial pattern to summer precipitation (Figure 2). Annual precipitation ranges from 17.1 at Lenghu in Q to 1769.8 at Emeishan in S. Annual maximum daily precipitation (unit: mm) spans from 6.5 at Lenghu to 119.6 at Emeishan (Figure 3b), with some of the lowest values also seen along the border of X (Qiemo, 8.9) and Q (Mangai, 9.2). The wet-season (May–September) CDDs (unit: days) range from 6.2 at Emeishan to 71.5 at Ruoqiang (Figure 3c). Drought persistence increases from the southeast to the northwest in Q and G, from the east to west in T, and from the northwest to southeast in X, but Y and S do not show a clear spatial gradient in CDDs (Figure 3c). The spatial pattern of annual and seasonal precipitation is related to the influence of the monsoon and westerlies that prevail in the region. The southeast is affected by the monsoon in summer that brings abundant moisture from the Indian Ocean and the South China Sea, whereas the northwest is farther away from the oceans and is also located in the leeward side of the Kunlun Mountains that causes the descending air to warm up and dry up under the influence of the westerlies.

3.2. Seasonal and Annual Trends

The trends of seasonal precipitation (unit: $mm \cdot y^{-1}$), ranging from −3.29 at Y's Zhanyi in summer to 3.01 at Y's Bomi in spring, display mixed signals spatiotemporally and a majority of the trends are not statistically significant (Figure 4). More positive trends than the combined negative and no trends show up in all seasons, but the southeast is becoming dry in autumn and to some extent in summer. The central and the northwestern TPS are evidently becoming wet. The trends of seasonal maximum daily precipitation (unit: $mm \cdot y^{-1}$; Figure 4) are largely similar spatially to those of seasonal precipitation except that the former shows more zero trends and fewer statistically significant trends than the latter, and that in autumn the former shows fewer negative trends over the southeast than the latter. This may indicate that the change of extreme precipitation is also the

reason of seasonal precipitation change in most areas of TPS. For seasonal maximum daily precipitation, the trends range from −0.60 at Yibin in summer to 0.31 at Zhaojue in winter in S. Seasonal CDD trends (unit: days·y^{-1}), ranging from −0.88 at Wuqiaoling in winter to 0.32 at Tieganlike in summer in X (Figure 4), are zero at a majority of the stations throughout the year. The spatial patterns of seasonal precipitation and maximum precipitation reveal some consistency in that increases (decreases) in precipitation tend to correspond to increases (decreases) in maximum daily precipitation. This suggests that maximum precipitation matters the most for seasonal precipitation as it appears that maximum precipitation contributes greatly to seasonal precipitation.
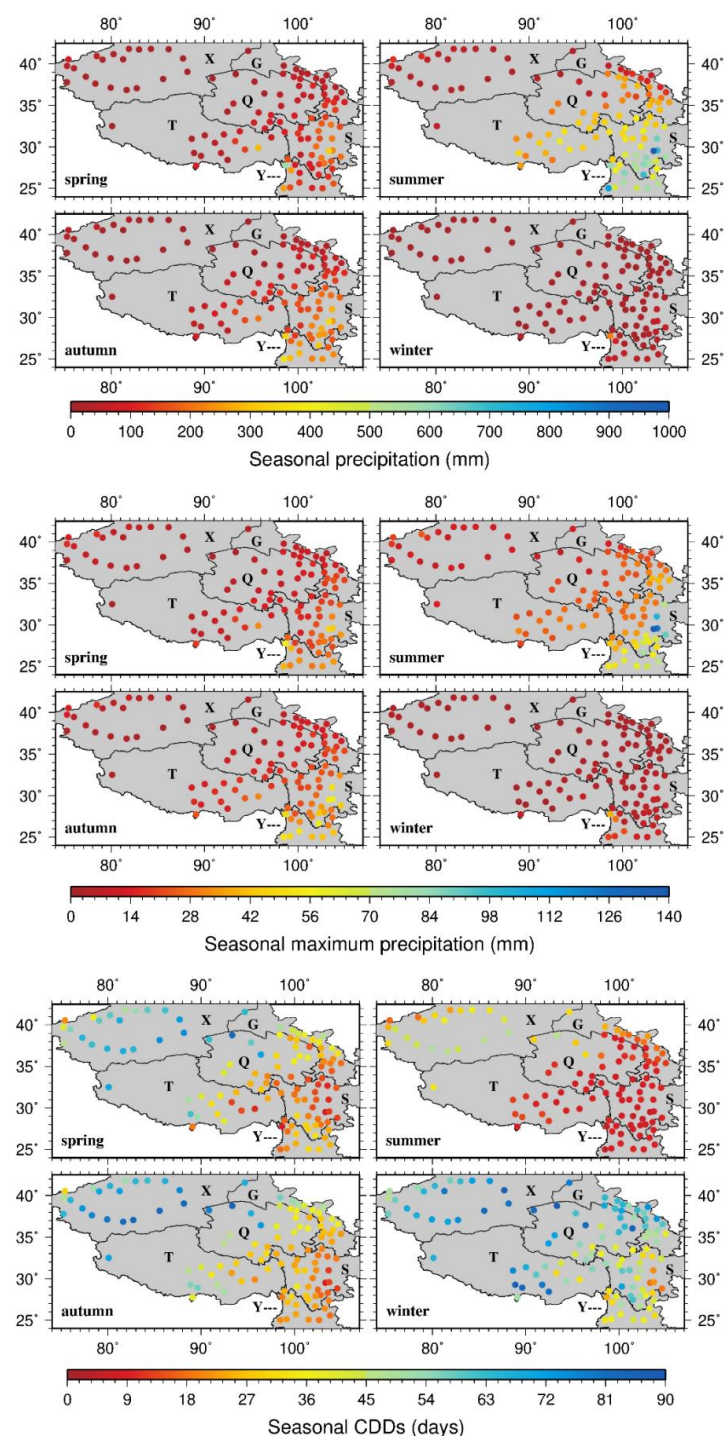
Figure 2. Spatial distributions of seasonal precipitation variables.
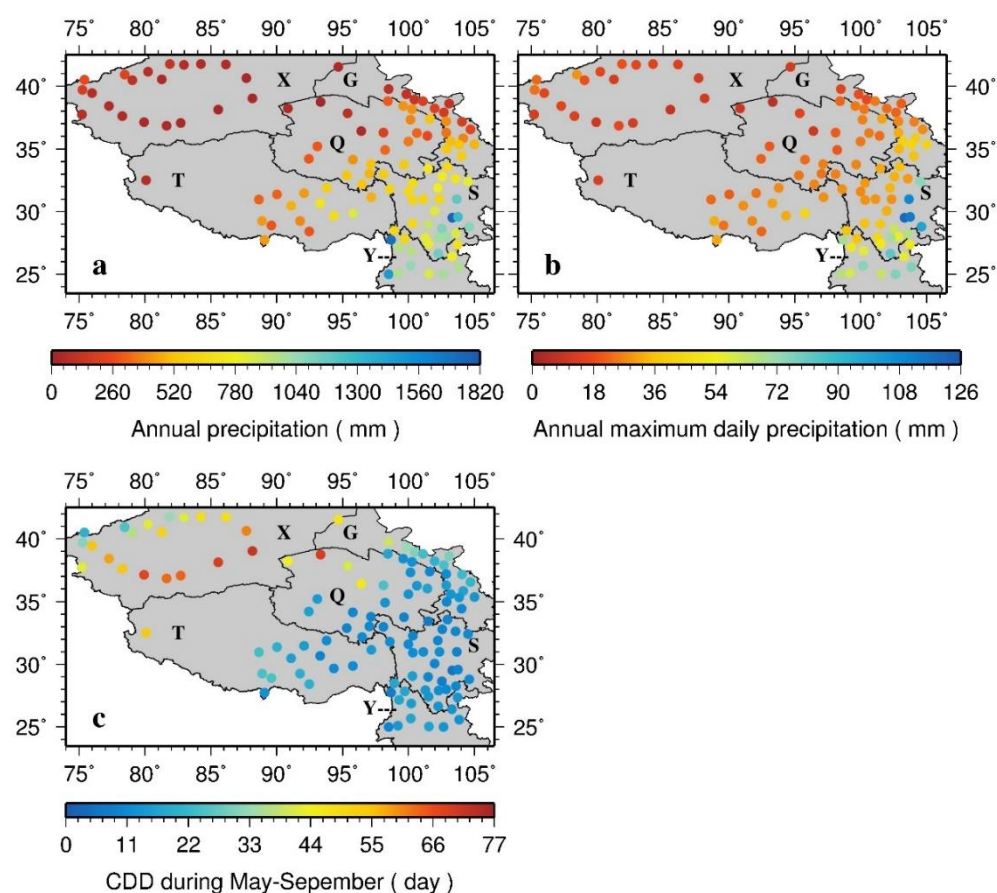
Figure 3. (**a**–**c**) Spatial distributions of annual precipitation variables.

Annual precipitation trends (units: mm·y^{-1}), mostly negative in the southeast but positive in the central and northwestern TPS (Figure 5a), closely follow the seasonal precipitation trends for summer (Figure 4), the peak precipitation season of the region. The greatest negative annual precipitation trends all appear in the eastern S. No statistically significant negative trends are seen in X, T, Q, G, and Y except for one station in G (Lingtao, −1.65) and Y (Zhanyi, −3.04). In all, annual precipitation at 37 (78) stations show negative (positive) trends and among them 7 (28) are statistically significant. Annual maximum daily precipitation trends (units: mm·y^{-1}), ranging from −0.58 at Yibin to 0.63 at Zhaojue in S and mainly negative in the southeastern but positive in the central and northwestern TPS (Figure 5b), display the same signs as those of annual precipitation at most of the stations. This further confirms that precipitation changes are due primarily to changes in extremes. For annual maximum daily precipitation, negative (positive) trends are seen at 40 (73) stations and most of the trends are not statistically significant. Trends of the wet-season CDDs (units: days·y^{-1}) range from −0.39 (Minfeng in X) to 0.31 (Tieganlike in X) (Figure 5c). There are 21 (18.2% of the total), 41 (35.7%), and 53 (46.1%) stations that show positive, negative, and zero trends, respectively. The zero trends distribute primarily in the southeast (i.e., 51 out of the 53 stations there with zero trends), so do the positive trends though to a lesser extent in number, while the negative trends are located mainly in the central and northwestern TPS. Both Figures 4 and 5 indicate that generally the southeast corresponds to small positive trends in CDDs and negative trends in precipitation and maximum daily precipitation while the opposite is true for the center and northwest. This suggests that the wet southeastern TPS is trending dry while the dry central and northwestern TPS are trending wet in the recent decades.
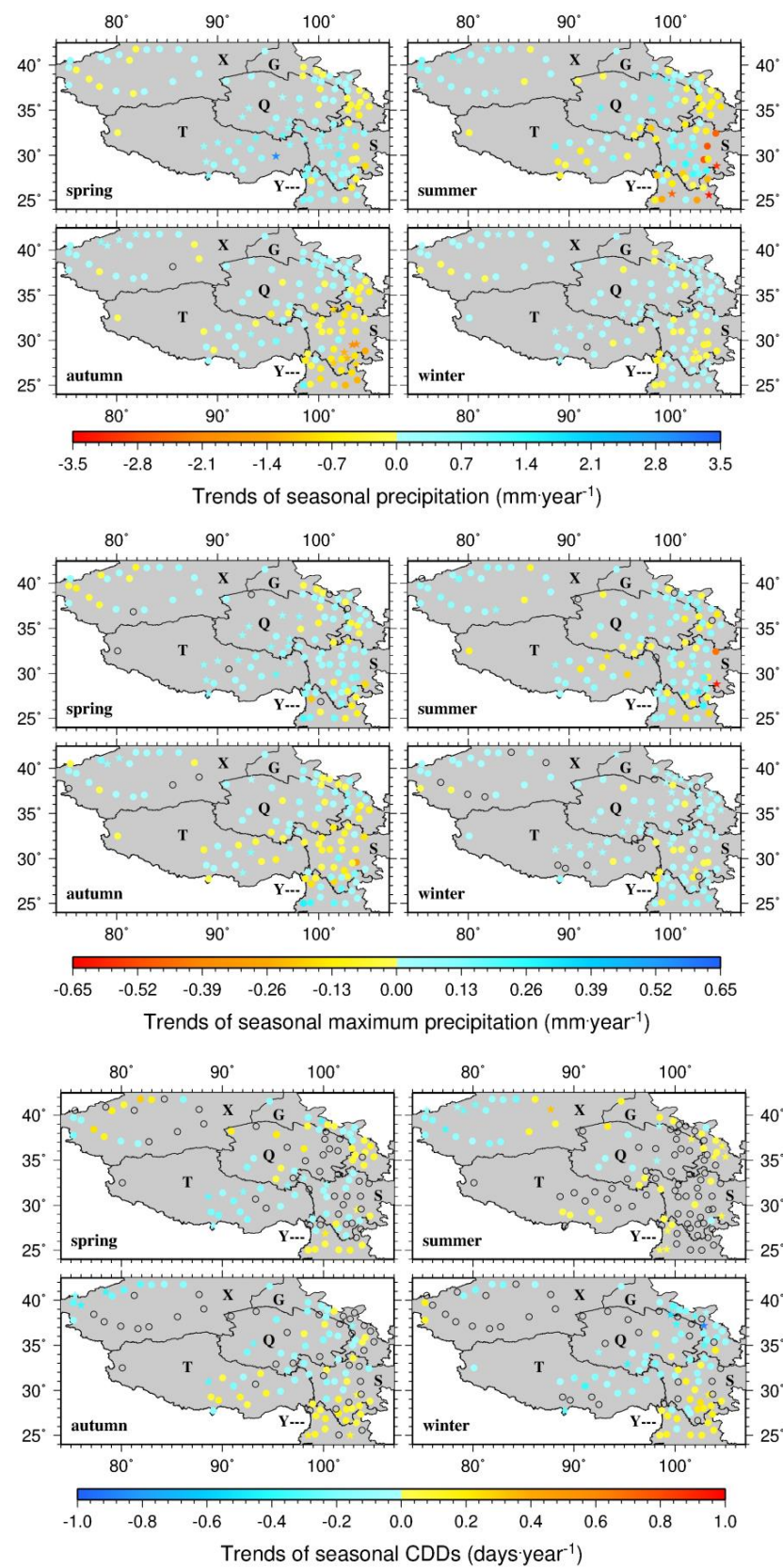
Figure 4. Spatial distributions of the trends of seasonal precipitation variables during 1963–2015. Stars represent statistically significant trends (*p* < 0.05). Open circles represent no trends.
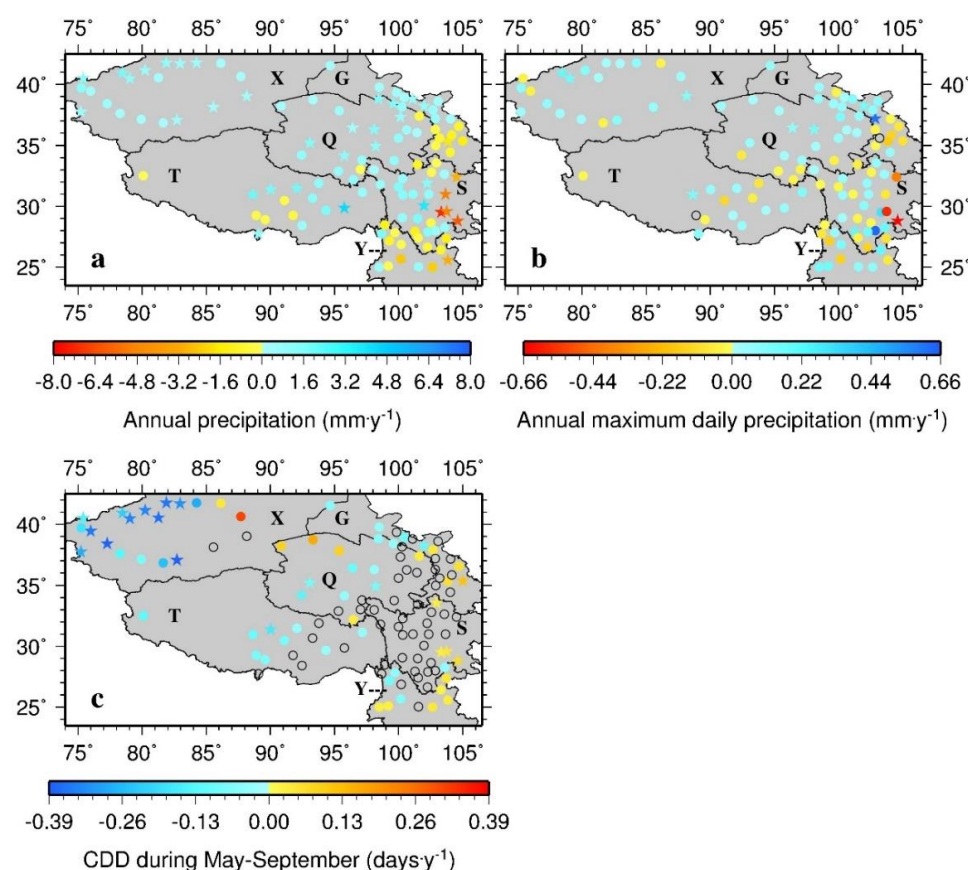
Figure 5. (**a**–**c**) Spatial distributions of the trends of annual precipitation variables during 1963–2015.

3.3. Precipitation and Its Trends in the River Basins

Mean seasonal and annual precipitation (unit: mm) in the 10 river basins is presented in Table 1. Notable variations can be seen among the 10 basins in seasonal precipitation. Seasonal precipitation ranges from 4.1 mm in winter in CTB and IDR to 463.7 mm in summer in YTR. Basins IDR and CTB have to be examined with caution since only 1 and 2 stations are located in IDR and CTB, respectively. Those basins that are located in the southeast (i.e., YTR, YLR, MKR, SWR) display considerably greater precipitation in summer than those located in the center and northwest (i.e., NQMB, CQB, TRB). However, in winter, differences in basin-averaged precipitation between the southeast and the center/northwest are rather small. This may suggest that in summer, there are large spatial variations in atmospheric conditions such as in the strength and extent of the monsoons and moisture while in winter, probably one dominant weather pattern such as the westerlies prevail over the TPS. Spring and autumn are transition seasons and in spring and autumn, MKR, SWR, YLR, and YTR consistently exhibit greater precipitation than the rest of the basins, due to their southeastern location with abundant moisture even in the relatively dry months. Annual precipitation totals from the wettest basin to the driest basin are 803.2, 708.2, 658.3, 543.6, 530.8, 315.2, 200.5, 130.0, 84.3, and 70.6 mm for YTR, MKR, SWR, YLR, BPR, CTB, NQMB, CQB, TRB, and IDR, respectively (Table 1).

Most trends of seasonal precipitation (unit: $mm \cdot y^{-1}$) over the 10 basins are not statistically significant (Table 1). Winter corresponds to rather small trends over the 10 basins, but in summer, the trends become greater in magnitude over the majority of the basins. Also in summer and winter, the basins located in the southeast, YTR, MKR, YLR, and SWR, all exhibit negative trends while the arid and semi-arid basins located in the center and northwest such as CQB, CTB, NQMB, and TRB all show positive trends. In fact, the arid and semi-arid basins display positive trends throughout the year. At the annual scale (Table 1), the trends are all statistically significant except for MKR and the

negative (positive) trends are noted for YTR, MKR, YLR, and IDR (CTB, BPR, NQMB, TRB, SWR, and CQB). All these are in line with the trends of seasonal and annual precipitation discussed earlier in that the southeast is trending dry while the center and northwest are trending wet in the wet season and annually.

As precipitation contributes greatly to the rivers on the TPS [4], the aforementioned changes in basin-averaged precipitation could have implications for water resources in the region. On the one hand, the drying tendency over the wet basins in the wet season poses challenges for the demand and supply of fresh water in the southeast as it is where a large portion of people live and also water is needed more in the wet season. As global warming progresses and the current trends continue, the drying tendency does not bode well for the southeast. On the other hand, the wetting tendency for the dry and semi-dry basins should be beneficial for the local population and ecosystems.

3.4. Recurrence Intervals of Extreme Daily Precipitation

The thresholds for the four recurrence periods, 20-year, 50-year, 100-year, and 200-year with the respective probability of 5%, 2%, 1%, and 0.5%, calculated using equation (6), show a similar spatial pattern of decreasing from the southeast to the northwest (Figure 6). This is consistent with the spatial patterns of annual precipitation and annual daily maximum precipitation (Figure 3). The lowest thresholds for all recurrence periods occur at Lenghu, the driest station, whereas the highest thresholds appear at Leshan, one of the wettest stations. The threshold ranges at the stations are 15.40–251.26 mm for the 20-year-event, 18.87–297.93 mm for the 50-year-event, 21.47–332.90 mm for the 100-year-even, and 24.05–367.74 mm for the 200-year-event, respectively.
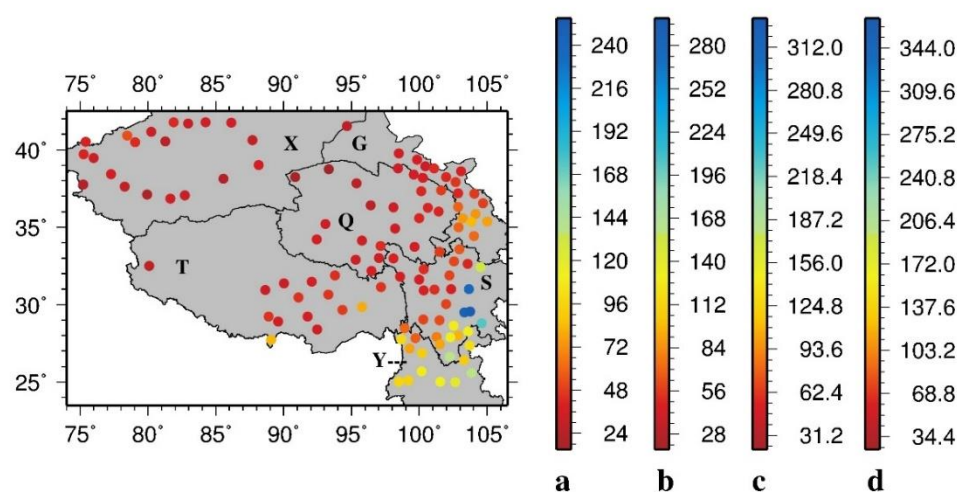

Figure 6. Thresholds of extreme daily precipitation for the 4 recurrence periods, 20-year (**a**), 50-year (**b**), 100-year (**c**), and 200-year (**d**) at the stations.

During 1963–2015, there are twenty 200-year extreme precipitation events (one in the 1960s; six in the 1970s and 1980s, respectively; two in the 1990s and 2000s, respectively; and three in the 2010s), eighteen 100-year events (five in the 1970s; six in the 1980s; four in the 1990s; two in the 2000s; and one in the 2010s), fifty-two 50-year events (3 in the 1960s; 9 in the 1970s, 1990s and 2000s, respectively; 11 in the 1980s and 2010s, respectively), and one hundred and fifty-four 20-year events (23 in the 1960s; 31 in the 1970s; 23 in the 1980s; 33 in the 1990s; 26 in the 2000s; and 18 in the 2010s) (Table S2 of the Supplementary Materials, Figure 7). Clearly, all four-category extreme precipitation events have happened in the past decades especially frequently in the 1970s and 1980s, but the greatest extreme precipitation events tend to occur after the late 1990s and in the southeastern TPS, for example, the 200-year event with 423.8 mm on 9 July 2013 at Dujiangyan in S, the 100-year event with 176.9 mm on 26 June 2009 at Zhanyi in Y, the 50-year event with 326.8 mm on 28 July 1996 at Leshan in S, and the 20-year event with 257.6 mm on 17 July 2010 at Leshan in S.
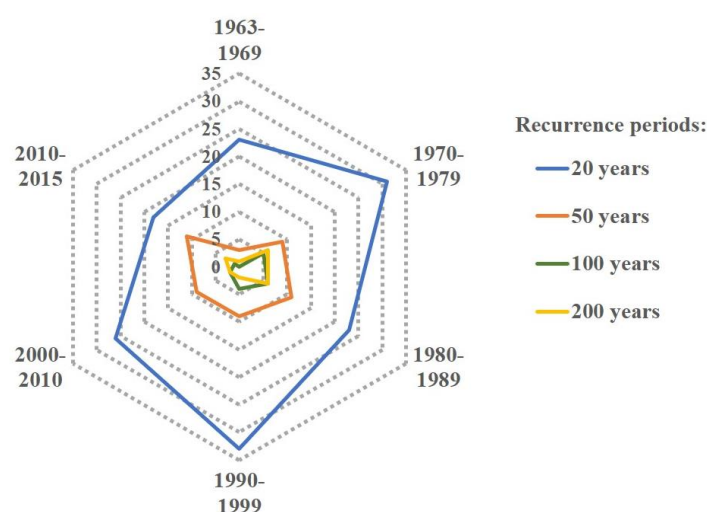
Figure 7. Number of extreme precipitation events for the four recurrence periods in different decades.

4. Discussions

Using station observations, we have shown that precipitation decreases from the southeast to the northwest on the TPS annually and in the wet season. In the dry season, precipitation is rather low across the TPS with little spatial variations. The spatial patterns of seasonal and annual maximum daily precipitation (CDDs) largely follow (oppose to) those of precipitation, decreasing (increasing) from the southeast to the northwest during the wet season and annually, but changing little during the dry season. Changes in precipitation extremes are largely responsible for changes in seasonal and annual precipitation. Also, the wet southeastern TPS is becoming dry while the dry central and northwestern TPS are becoming wet in the recent decades generally. In an attempt to explain the identified changes in precipitation and its extremes on the TPS, we examine the relationships of precipitation with climate systems and investigate the spatiotemporal patterns of water vapor and atmospheric stability in the following.

4.1. Correlations of Precipitation with Climate Systems

The seasonal trends of the indices of the climate systems over 1963–2015 that directly and indirectly affect the TPS are listed in Table 3. ISM and WNPM show statistically insignificant negative trends in summer. For WJ, spring, autumn, and winter (summer) correspond to positive (negative) trends with statistical significance noted for winter only. ENSO exhibits positive (negative) trends for spring, summer, and autumn (winter) that are not statistically significant. NAO displays positive trends in spring and winter and negative trends in summer and autumn, and significance is noted for summer and winter. The trends of TH are all positive and all significant. Among these climate systems, the monsoons, westerly jet, and Tibetan Plateau High more directly impact the TPS, while ENSO and NAO exert indirect influence on the TPS.

Table 3. Seasonal trends of climate system indices. Bold fonts represent statistically significant trends ($p < 0.05$).

	ISM	WNPM	WJ	ENSO	NAO	TH
spring			0.0185	0.0114	0.0064	**2.2503**
summer	−0.0090	−0.0006	−0.0059	0.0137	**−0.0186**	**2.4487**
autumn			0.0111	0.0034	−0.0055	**2.9216**
winter			**0.0539**	−0.0008	**0.0241**	**2.6635**

We employ the nonparametric Spearman correlation analysis [57,58] to identify the degree of correlation between precipitation variables at every station and the indices of climate systems. We focus on the monsoons and westerly jet as these two systems are

documented to affect the region in a non-trivial way [26,59–62], but we have also computed and presented the correlations of precipitation variables with all other indices. Furthermore, we focus on the correlation of seasonal precipitation with the indices as seasonal maximum daily precipitation and CDD exhibit the similar patterns to those of seasonal precipitation though with fewer statistically significant correlation coefficients.

In Summer, precipitation correlates positively (negatively) with ISM over the western and southern S (Figure 8) where precipitation shows increase trends (Figure 4). Also, generally positive correlation can be seen over the central to northwestern TPS (Figure 8) where precipitation mainly increases (Figure 4). This means that the insignificantly weakening ISM will not be able to explain the precipitation increase in those areas. The exception is over Y and the southeast G where positive correlation and decreasing precipitation are noted, suggesting that the decreasing trends in precipitation may be due to the weakening ISM. WNPM also displays insignificantly weakening trends in summer (Table 3) and generally positive (negative) correlation is seen where precipitation exhibits increase (decrease) trends (Figure 8 vs. Figure 4). Thus, WNPM also will not be able to explain the precipitation trends on the TPS.
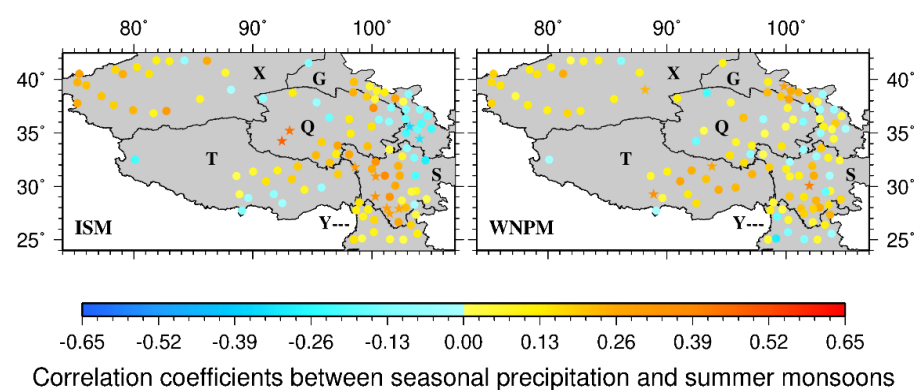
Figure 8. Spatial distributions of correlation coefficients between seasonal precipitation and summer monsoon. Stars represent statistically significant trends ($p < 0.05$). Open circles denote zero correlations. The same notation applies in the following figures as well.

In spring and autumn for which WJ strengthens slightly (Table 3), the positive correlation of precipitation with WJ generally corresponds to an increase in precipitation trends near the border of T, S and Y in spring and majority stations in X, Q and G in winter (Figure 9 vs. Figure 4), suggesting that WJ may account for the precipitation trends in those areas to some extent. In summer, WJ weakens slightly (Table 3) but there is general increase (decrease) in precipitation trends over the majority (eastern and southeastern) stations in the TPS, and there are significant positive correlation near the border of Q, T and S (Figures 4 and 9), which means that WJ will not be able to explain the precipitation trends in summer. On the other hand, WJ strengthens significantly in winter (Table 3) and a mainly positive correlation is seen over the central to northwestern TPS (Figure 9) where precipitation increases (Figure 4), indicating the importance of WJ in explaining the precipitation trends there.

ENSO is characterized by seasonal phase locking, stronger in winter and weaker in summer, and ENSO shows little trends in winter (Table 3). The correlation of precipitation with ENSO is predominantly positive in the south but negative in the east in winter (Figure 9). NAO trends are significantly positive in winter (Table 3) and precipitation correlates mainly positively with NAO over the TPS in winter (Figure 10). In summer, NAO trends are strongly negative (Table 3) and, except for a few stations, there is good correspondence of a positive (negative) correlation with the increase (decrease) of precipitation across the TPS (Figures 4 and 10). Thus, NAO appears to somewhat explain the wetting trend in the central and northwestern TPS in winter and the drying trend in the southeastern TPS in summer.
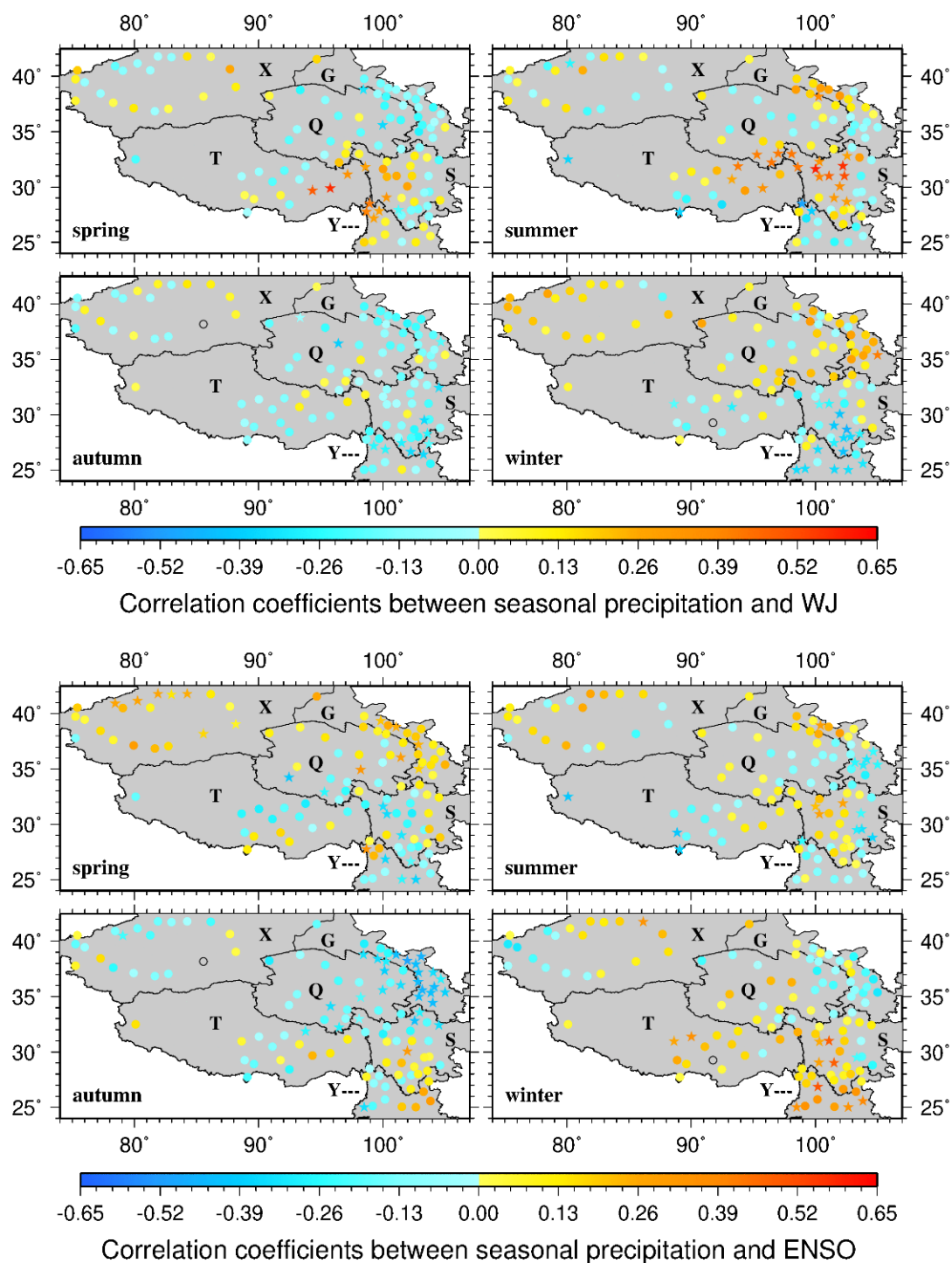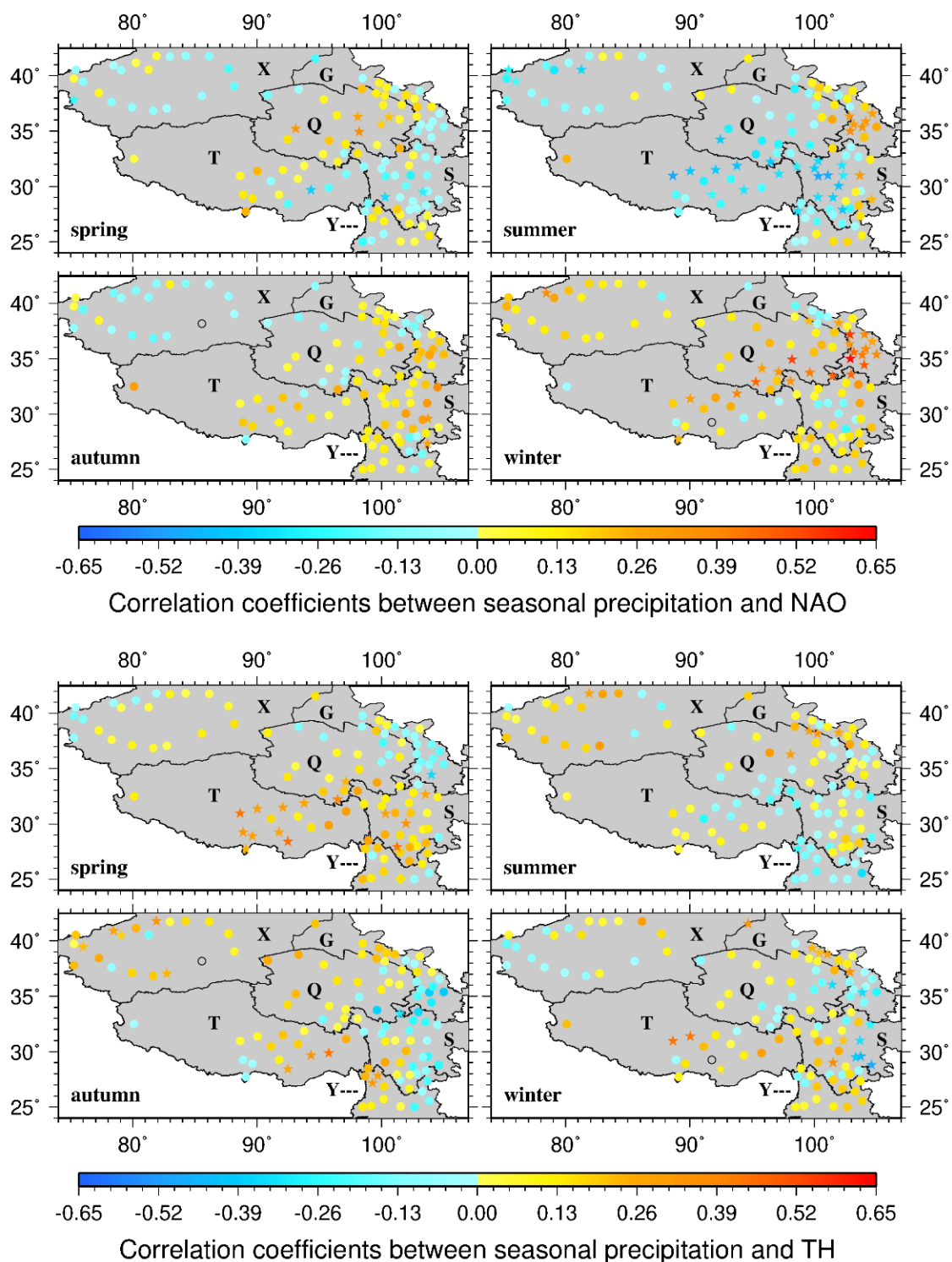
Figure 9. Spatial distributions of correlation coefficients between monthly precipitation and WJ and ENSO. Stars represent statistically significant trends (*p* < 0.05). Open circles denote zero correlations.

TH is the only index among all the indices that shows statistically significant positive trends throughout the year (Table 3). This indicates that the Tibetan Plateau High is strengthening and the result of this strengthening would be increased sinking (rising) motion over the area of its direct influence (its peripheries). The correlation of precipitation with TH shows large spatial heterogeneity, with a positive correlation noted over the central TPS in spring and a negative correlation in Y in summer (Figure 10). This pattern, however, does not help to explain the drying trend in the central and northwestern TPS and the wetting trend in the southeastern TPS.

Figure 10. Spatial distributions of correlation coefficients between monthly precipitation and NAO and TH. Stars represent statistically significant trends (*p* < 0.05). Open circles denote zero correlations.

It is clear from the above analyses that precipitation changes on the TPS cannot be fully attributed to a particular system or systems and that disentangling the impact of one climate system from another is difficult since the systems are working collectively in a dynamic way. It appears that (1) the drying trends in Y in summer may be due to weakening ISM and weakening NAO, and (2) the wetting trends in the central and northwestern TPS in winter may be related to strengthening WJ and strengthening NAO. Furthermore, the local complex terrain could have also played a role in shaping the spatially heterogeneous

precipitation changes. One example is the west-east dipole structure over S that can often be identified in the precipitation and correlation patterns in summer. Such a pattern is apparently related to the two geographically distinct parts of S: The relatively flat and low-elevation eastern part and the mountainous and high-elevation western part.

4.2. Patterns and Changes of Water Vapor

One of the key elements for precipitation generation and development is water vapor. Due to the primarily dry climate over the TPS, water vapor transport from outside of the TPS is critical [63]. The strength and direction of water vapor transport and their variations thus determine the distribution and variations of precipitation over the TPS. In this section, we use the ERA5 reanalysis data to explore the connection of precipitation and its changes with water vapor transport.

Annual and seasonal precipitation and changes at the station locations and at the ERA5 grids encompassing the TPS are compared in Figure S1 of the Supplementary Materials. ERA5 resolves the observed southeast to northwest gradient in precipitation and the drying trends in the southeast and the wetting trends in the center reasonably well. Major discrepancies include (1) ERA5 showing mainly wetting trends while the observations display drying trends over X and (2) the observed magnitude of precipitation amount and trends being generally overestimated by ERA5. These discrepancies could be related to several factors including deficiencies in ERA5 forcing and physics schemes [64,65] as well as a lack of observations on the TPS for data assimilation and for model evaluation. Complex terrain also complicates climate modeling and reanalysis over the TPS [63]. Despite the differences, the generally satisfactory performance of ERA5 in resolving the observed distributions of precipitation and trends over the TPS lends credence to using the reanalysis to investigate the relationship between precipitation and water vapor.

Spatial distributions of the means and trends of ERA5 total column water vapor (TCWV) are presented in Figure 11. There exists a clear southeast-northwest gradient in TCWV seasonal means especially in summer that corresponds well to that of precipitation. Elevated TCWV is seen over X in all seasons compared to the central TPS, likely contributing to the overestimation of the observed precipitation in X. TCWV decreases over the eastern S and Y but increases over the central TPS in nearly all seasons, largely consistent with the drying trends in the southeast and the wetting trends in the center.

What might be the reason for decreasing TCWV over the southeast and increasing TCWV over the center? For the TPS, moisture comes mainly from the south related to the southerly flow and secondarily from the west related to the westerly flow [66]. At 500 hPa (and similarly at 600 hPa), which is close to low level given the averaged 4000-m elevation of the TPS, Y, S, and T are under the influence of the southerly (Figure 12, Figure S2 of the Supplementary Materials) and westerly (Figures S3 and S4 of the Supplementary Materials) in all seasons. Both the southerly and westerly are weakening over Y and S in summer and autumn (Figure 12 and Figures S2–S4), which clearly bring less moisture to the southeast and contribute to the drying there. On the other hand, over the central TPS at 500 hPa that is controlled mainly by the westerly (Figures S3 and S4), the strengthening of the westerly in autumn and especially in winter could increase the moisture transport to the area and contribute to the wetting trends there. The strengthening of the westerly over the central TPS in winter is clearly related to the northward shift of the 200-hPa East Asian jet stream (Figure 13).

The above analyses are consistent with what the vertical integrals of northward water vapor flux (Figure S5 of the Supplementary Materials) and eastward vapor flux (Figure S6 of the Supplementary Materials) reveal. Specifically, decreasing trends in both fluxes are seen over the southeast in summer and autumn while increasing trends in both fluxes are seen over the TPS in winter and over the central to northwestern TPS in summer and autumn. The weakening of the southerly and westerly in the southeast in summer is consistent with the weakening of the Asian summer monsoons and the westerly jet while

the strengthening of the westerly over the TPS in winter is in line with the strengthening of the wester jet (Table 3).
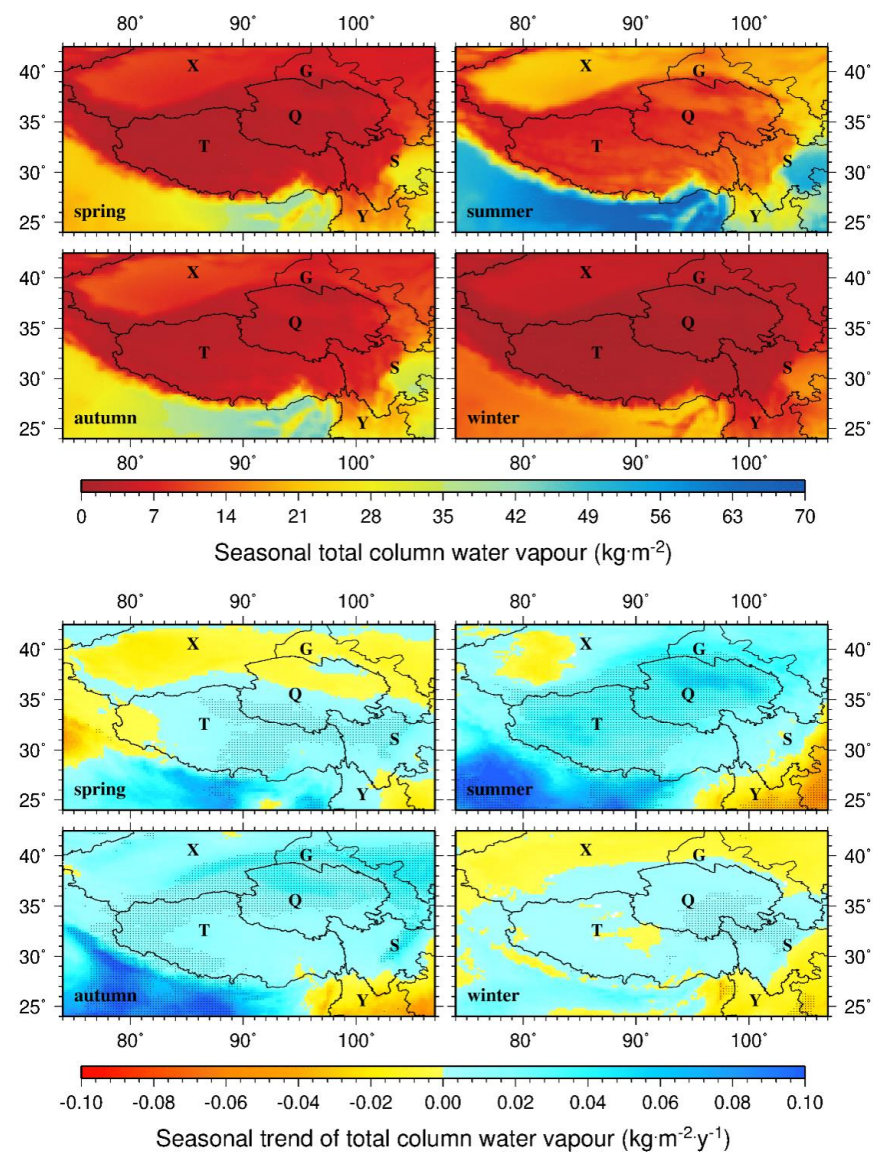

Figure 11. Spatial distributions of the means and trends of ERA5 total column water vapor (TCWV) during 1979–2015. Statistically significant trends (*p* < 0.05) are represented by crosses in this figure and the following figures.

4.3. Patterns and Changes of Atmospheric Instability

Atmospheric instability, for which convective available potential energy (CAPE) is a good indicator, is another key element for precipitation to develop. The spatial patterns of the means and trends of EAR5 CAPE presented in Figure 14 show elevated CAPE primarily to the south of the Himalayas but large spatial variations in the trends. Clearly, CAPE decreases over the southeast in spring, summer, and winter and to a lesser extent in autumn while increases over the center in summer, autumn, and winter and to a lesser extent in spring (Figure 14). Such a pattern in the CAPE trends is conducive to the drying trends in the southeast and the wetting trends in the center. It is difficult though to pinpoint what may have caused the spatially varying trends in CAPE over the TPS. We have examined the sub-area averaged vertical temperature profiles and their trends (not shown) but have not identified clear indications of temperature changes in the vertical.
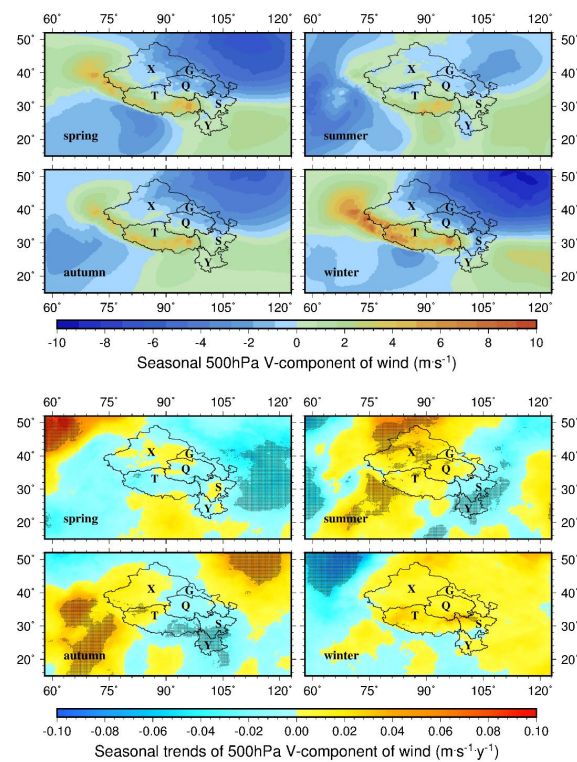
Figure 12. Spatial distributions of the means and trends of V-component wind at 500 hPa (Vcw500) during 1979–2015. Negative values represent southward wind.
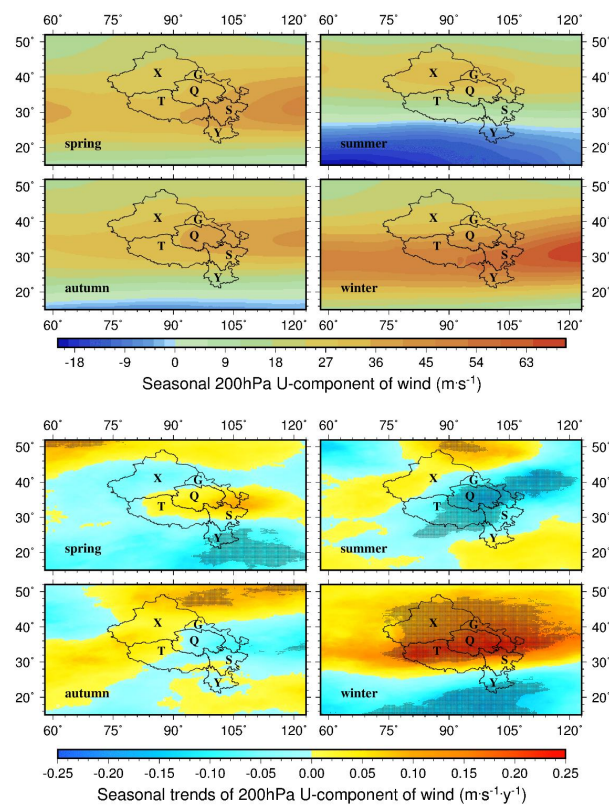

Figure 13. Spatial distributions of the means and trends of U-component wind at 200 hPa (Ucw200) during 1979–2015. Negative values represent westward wind.
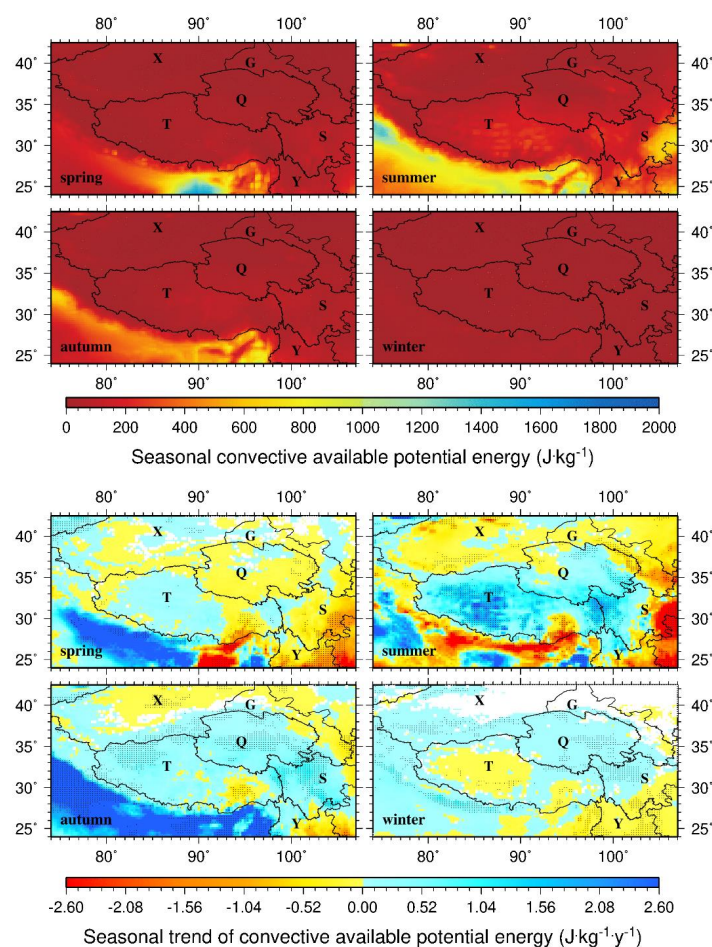
Figure 14. Spatial distributions of the means and trends of ERA5 CAPE during 1979–2015.

5. Conclusions

In this study, the daily precipitation data from 115 weather stations during 1963–2015 are employed to investigate precipitation and its wet and dry extremes at seasonal and annual time scales over the TPS. The recurrence periods of extreme daily precipitation at the stations are also examined. The mechanisms of seasonal precipitation changes are further investigated using atmospheric circulation indices and moisture transports and atmospheric instability from the ERA5 reanalysis. The major findings are summarized as follows.

1. There exists a clear southeast-northwest precipitation gradient in the TPS. The wettest and driest stations on the TPS are Emeishan in S and Lenghu in Q, respectively. Maximum daily precipitation shows a similar pattern to that of precipitation at seasonal and annual time scales, while the consecutive dry days (CDDs) exhibit a nearly opposite pattern to that of precipitation.
2. The wet southeastern TPS generally corresponds to little or small positive trends in CDDs and negative trends in precipitation and maximum daily precipitation during most of the seasons and at annual time scale while the opposite is true for the dry central and northwestern TPS. This suggests that the wet southeast is trending dry while the dry center and northwest are trending wet in 1963–2015. Also, increases (decreases) in precipitation tend to correspond to increases (decreases) in maximum daily precipitation but decreases (increases) in CDDs, which suggest that it is the extremes daily precipitation that matter the most.
3. The drying tendency over the wet basins in the southeast in the wet season and wetting tendency over the dry and semi-dry basins in the center and northwest could have some implications for water resources in the region. The drying tendency in the

wet basins would reduce the supply of fresh water in the wet season when water is especially needed while the wetting tendency in the dry and semi-dry basins would benefit the watersheds.

4. The thresholds for the 20-year, 50-year, 100-year, and 200-year recurrence periods decrease from the southeast to the northwest, consistent with the spatial patterns of annual precipitation and annual maximum daily precipitation. The highest thresholds for all recurrence periods occur at Leshan, one of the wettest stations, whereas the lowest thresholds appear at Lenghu, one of the driest stations. The greatest extreme precipitation events tend to occur after the late 1990s and in the southeastern TPS.

5. The climate systems that directly and indirectly impact the TPS appear to work collectively in a dynamic way and precipitation changes on the TPS cannot be fully attributed to one climate system. What seems clear is that (1) moisture transports to the southeast from the south and the west are weakened in summer due to the weakening of the southerly/westerly as related to the weakening of the summer monsoons/the westerly jet; (2) moisture transports to the center are strengthened in winter due to the strengthening of the westerly jet and NAO; and (3) decreased instability over the southeast and increased instability over the center are conducive to the drying trends in the southeast and the wetting trends in the center. NAO and topography also seem to play some roles in precipitation changes over the TPS.

Author Contributions: Data curation, J.D. and C.Z.; Methodology, L.C., L.L. and Z.L.; Supervision, Y.Z.; Visualization, J.D.; Writing—original draft, J.D.; Writing—review & editing, J.D., L.C. and Y.Z. All authors have read and agreed to the published version of the manuscript.

Institutional Review Board Statement: Not applicable.

Informed Consent Statement: Not applicable.

Data Availability Statement: Not applicable.

Conflicts of Interest: The authors declare no conflict of interest.

References

1. Li, X.; Jin, R.; Pan, X.; Zhang, T.; Guo, J. Changes in the near-surface soil freeze–thaw cycle on the Qinghai-Tibetan Plateau. *Int. J. Appl. Earth Obs. Geoinf.* **2012**, *17*, 33–42. [CrossRef]
2. Cuo, L.; Zhang, Y.; Gao, Y.; Hao, Z.; Cairang, L. The impacts of climate change and land cover/use transition on the hydrology in the upper Yellow River Basin, China. *J. Hydrol.* **2013**, *502*, 37–52. [CrossRef]
3. Cuo, L.; Zhang, Y.; Wang, Q.; Zhang, L.; Zhou, B.; Hao, Z.; Su, F. Climate Change on the Northern Tibetan Plateau during 1957–2009: Spatial Patterns and Possible Mechanisms. *J. Clim.* **2013**, *26*, 85–109. [CrossRef]
4. Cuo, L.; Zhang, Y.; Zhu, F.; Liang, L. Characteristics and changes of streamflow on the Tibetan Plateau: A review. *J. Hydrol. Reg. Stud.* **2014**, *2*, 49–68. [CrossRef]
5. Shen, W.; Zou, C.; Liu, D.; Ouyang, Y.; Zhang, H.; Yang, C.; Bai, S.; Lin, N. Climate-forced ecological changes over the Tibetan Plateau. *Cold Reg. Sci. Technol.* **2015**, *114*, 27–35. [CrossRef]
6. Yan, L.; Zheng, M. The response of lake variations to climate change in the past forty years: A case study of the northeastern Tibetan Plateau and adjacent areas, China. *Quat. Int.* **2015**, *371*, 31–48. [CrossRef]
7. Zheng, Z.; Zhu, W.; Chen, G.; Jiang, N.; Fan, D.; Zhang, D. Continuous but diverse advancement of spring-summer phenology in response to climate warming across the Qinghai-Tibetan Plateau. *Agric. For. Meteorol.* **2016**, *223*, 194–202. [CrossRef]
8. Zhu, F.; Cuo, L.; Zhang, Y.; Luo, J.-J.; Lettenmaier, D.P.; Lin, Y.; Liu, Z. Spatiotemporal variations of annual shallow soil temperature on the Tibetan Plateau during 1983–2013. *Clim. Dyn.* **2017**, *51*, 2209–2227. [CrossRef]
9. Tian, L.; Masson-Delmotte, V.; Stievenard, M.; Yao, T.; Jouzel, J. Tibetan Plateau summer monsoon northward extent revealed by measurements of water stable isotopes. *J. Geophys. Res. Space Phys.* **2001**, *106*, 28081–28088. [CrossRef]
10. Zhang, Y.; Enomoto, H.; Ohata, T.; Kitabata, H.; Kadota, T.; Hirabayashi, Y. Glacier mass balance and its potential impacts in the Altai Mountains over the period 1990–2011. *J. Hydrol.* **2017**, *553*, 662–677. [CrossRef]
11. Cuo, L.; Zhang, Y. Spatial patterns of wet season precipitation vertical gradients on the Tibetan Plateau and the surroundings. *Sci. Rep.* **2017**, *7*, 1–10. [CrossRef]
12. Ding, J.; Cuo, L.; Zhang, Y.; Zhu, F. Monthly and annual temperature extremes and their changes on the Tibetan Plateau and its surroundings during 1963–2015. *Sci. Rep.* **2018**, *8*, 1–23. [CrossRef]
13. Lin, Z.; Zhao, X. Spatial characteristics of changes in temperature and precipitation of the Qinghai-Xizang (Tibet) plateau. *Sci. China Earth Sci.* **1996**, *39*, 442–448. [CrossRef]
14. You, Q.; Kang, S.; Aguilar, E.; Yan, Y. Changes in daily climate extremes in the eastern and central Tibetan Plateau during 1961–2005. *J. Geophys. Res. Space Phys.* **2008**, *113*, 1639–1647. [CrossRef]
15. Ge, G.; Shi, Z.; Yang, X.; Hao, Y.; Guo, H.; Kossi, F.; Xin, Z.; Wei, W.; Zhang, Z.; Zhang, X.; et al. Analysis of Precipitation Extremes in the Qinghai-Tibetan Plateau, China: Spatio-Temporal Characteristics and Topography Effects. *Atmosphere* **2017**, *8*, 127. [CrossRef]
16. Wang, Y.; Liao, W.; Ding, Y.; Wang, X.; Jiang, Y.; Song, X.; Lei, X. Water resource spatiotemporal pattern evaluation of the upstream Yangtze River corresponding to climate changes. *Quat. Int.* **2015**, *380–381*, 187–196. [CrossRef]
17. Tian, Q.; Prange, M.; Merkel, U. Precipitation and temperature changes in the major Chinese river basins during 1957–2013 and links to sea surface temperature. *J. Hydrol.* **2016**, *536*, 208–221. [CrossRef]
18. Jiang, C.; Zhang, L.; Tang, Z. Multi-temporal scale changes of streamflow and sediment discharge in the headwaters of Yellow River and Yangtze River on the Tibetan Plateau, China. *Ecol. Eng.* **2017**, *102*, 240–254. [CrossRef]
19. Wu, F.; Wang, X.; Cai, Y.; Li, C. Spatiotemporal analysis of precipitation trends under climate change in the upper reach of Mekong River basin. *Quat. Int.* **2016**, *392*, 137–146. [CrossRef]
20. Yang, Y.; Jun, D.U.; Luo, S.X.; Shi, L. On extreme precipitation events in the Nujiang river basin in Tibet in recent 40 years. *Arid Zone Res.* **2013**, *30*, 315–321. (In Chinese) [CrossRef]
21. Deng, H.; Chen, Y. Influences of recent climate change and human activities on water storage variations in Central Asia. *J. Hydrol.* **2017**, *544*, 46–57. [CrossRef]
22. Song, C.; Huang, B.; Ke, L.; Ye, Q. Precipitation variability in High Mountain Asia from multiple datasets and implication for water balance analysis in large lake basins. *Glob. Planet. Chang.* **2016**, *145*, 20–29. [CrossRef]
23. Wu, C.; Hu, B.X.; Huang, G.; Zhang, H. Effects of climate and terrestrial storage on temporal variability of actual evapotranspiration. *J. Hydrol.* **2017**, *549*, 388–403. [CrossRef]
24. Sun, H.; Su, F.; Huang, J.; Yao, T.; Luo, Y.; Chen, D. Contrasting precipitation gradient characteristics between westerlies and monsoon dominated upstream river basins in the Third Pole. *Chin. Sci. Bull.* **2019**, *65*, 91–104. (In Chinese) [CrossRef]
25. Liu, X.; Yin, Z.-Y. Spatial and Temporal Variation of Summer Precipitation over the Eastern Tibetan Plateau and the North Atlantic Oscillation. *J. Clim.* **2001**, *14*, 2896–2909. [CrossRef]
26. Zhang, Y.; Li, T.; Wang, B. Decadal Change of the Spring Snow Depth over the Tibetan Plateau: The Associated Circulation and Influence on the East Asian Summer Monsoon. *J. Clim.* **2004**, *17*, 2780–2793. [CrossRef]
27. Tian, L.; Yao, T.; MacClune, K.; White, J.W.C.; Schilla, A.; Vaughn, B.; Vachon, R.; Ichiyanagi, K. Stable isotopic variations in west China: A consideration of moisture sources. *J. Geophys. Res. Space Phys.* **2007**, *112*. [CrossRef]
28. Zhang, Q.; Xu, C.-Y.; Jiang, T.; Wu, Y. Possible influence of ENSO on annual maximum streamflow of the Yangtze River, China. *J. Hydrol.* **2007**, *333*, 265–274. [CrossRef]

29. Wu, Z.; Li, J.; Jiang, Z.; Ma, T. Modulation of the Tibetan Plateau Snow Cover on the ENSO Teleconnections: From the East Asian Summer Monsoon Perspective. *J. Clim.* **2012**, *25*, 2481–2489. [CrossRef]

30. Wang, H.; Chen, Y.; Li, W. Characteristics in streamflow and extremes in the Tarim River, China: Trends, distribution and climate linkage. *Int. J. Clim.* **2014**, *35*, 761–776. [CrossRef]

31. Wang, H.; Chen, Y.; Pan, Y. Characteristics of drought in the arid region of northwestern China. *Clim. Res.* **2015**, *62*, 99–113. [CrossRef]

32. Li, B.; Chen, Y.; Chen, Z.; Xiong, H.; Lian, L. Why does precipitation in northwest China show a significant increasing trend from 1960 to 2010? *Atmos. Res.* **2016**, *167*, 275–284. [CrossRef]

33. Jiang, X.; Ting, M. A Dipole Pattern of Summertime Rainfall across the Indian Subcontinent and the Tibetan Plateau. *J. Clim.* **2017**, *30*, 9607–9620. [CrossRef]

34. Wang, B.; Fan, Z. Choice of South Asian Summer Monsoon Indices. *Bull. Am. Meteorol. Soc.* **1999**, *80*, 629–638. [CrossRef]

35. Wang, B.; Wu, R.; Lau, K.-M. Interannual variability of asian summer monsoon: Contrast between the indian and western north pacific-east asian monsoons. *J. Clim.* **2001**, *14*, 4073–4090. [CrossRef]

36. Duan, A.; Wu, G. Weakening Trend in the Atmospheric Heat Source over the Tibetan Plateau during Recent Decades. Part II: Connection with Climate Warming. *J. Clim.* **2009**, *22*, 4197–4212. [CrossRef]

37. Hersbach, H.; Dee, D. "ERA-5 Reanalysis in Production", ECMWF Newsletter, Number 147. Spring 2016. Available online: https://www.ecmwf.int/en/newsletter/147/news/era5-reanalysis-production (accessed on 11 May 2021).

38. Dee, D.P.; Uppala, S.M.; Simmons, A.J.; Berrisford, P.; Poli, P.; Kobayashi, S.; Andrae, U.; Balmaseda, M.A.; Balsamo, G.; Bauer, P.; et al. The ERA-Interim reanalysis: Configuration and performance of the data assimilation system. *Q. J. R. Meteorol. Soc.* **2011**, *137*, 553–597. [CrossRef]

39. Albergel, C.; Dutra, E.; Munier, S.; Calvert, J.-C.; Munoz-Sabater, J.; de Rosnay, P.; Balsamo, G. ERA-5 and ERA-Interim driven ISBA land surface model simulations: Which one performs better? *Hydrol. Earth Syst. Sci.* **2018**, *22*, 3515–3532. [CrossRef]

40. Mann, H.B. Nonparametric tests against trend. *Econometrica* **1945**, *13*, 245–259. [CrossRef]

41. Kendall, M.G. *Rank Correlation Methods*; Griffin: London, UK, 1975.

42. Cannarozzo, M.; Noto, L.; Viola, F. Spatial distribution of rainfall trends in Sicily (1921–2000). *Phys. Chem. Earth, Parts A/B/C* **2006**, *31*, 1201–1211. [CrossRef]

43. Guhathakurta, P.; Sreejith, O.P.; A Menon, P. Impact of climate change on extreme rainfall events and flood risk in India. *J. Earth Syst. Sci.* **2011**, *120*, 359–373. [CrossRef]

44. Tabari, H.; Talaee, P.H. Temporal variability of precipitation over Iran: 1966–2005. *J. Hydrol.* **2011**, *396*, 313–320. [CrossRef]

45. Sen, P.K. Estimates of the regression coefficient based on Kendall's Tau. *J. Am. Stat. Assoc.* **1968**, *63*, 1379–1389. [CrossRef]

46. Gumbel, E.J. *Statistics of Extremes*; Columbia University Press: New York, NY, USA, 1958.

47. Waylen, P.; Woo, M.-K. Prediction of annual floods generated by mixed processes. *Water Resour. Res.* **1982**, *18*, 1283–1286. [CrossRef]

48. Caporali, E.; Cavigli, E.; Petrucci, A. The index rainfall in the regional frequency analysis of extreme events in Tuscany (Italy). *Environmetrics* **2008**, *19*, 714–724. [CrossRef]

49. Strupczewski, W.G.; Kochanek, K.; Bogdanowicz, E.; Markiewicz, I. On seasonal approach to flood frequency modelling. Part I: Two-component distribution revisited. *Hydrol. Process.* **2011**, *26*, 705–716. [CrossRef]

50. Gu, X.; Zhang, Q.; Singh, V.P.; Shi, P. Non-stationaries in the occurrence rate of heavy precipitation across China and its relationship to climate teleconnection patterns. *Int. J. Clim.* **2017**, *37*, 4186–4198. [CrossRef]

51. Rahimzadeh, F.; Asgari, A.; Fattahi, E. Variability of extreme temperature and precipitation in Iran during recent decades. *Int. J. Clim.* **2009**, *29*, 329–343. [CrossRef]

52. Zhang, X.; Alexander, L.V.; Hegerl, G.C.; Jones, P.; Tank, A.K.; Peterson, T.C.; Trewin, B.; Zwiers, F.W. Indices for monitoring changes in extremes based on daily temperature and precipitation data. *Wiley Interdiscip. Rev. Clim. Chang.* **2011**, *2*, 851–870. [CrossRef]

53. Hu, Z.; Li, Q.; Chen, X.; Teng, Z.; Chen, C.; Yin, G.; Zhang, Y. Climate changes in temperature and precipitation extremes in an alpine grassland of Central Asia. *Theor. Appl. Clim.* **2016**, *126*, 519–531. [CrossRef]

54. Dosio, A. Projections of climate change indices of temperature and precipitation from an ensemble of bias-adjusted high-resolution EURO-CORDEX regional climate models. *J. Geophys. Res. Atmos.* **2016**, *121*, 5488–5511. [CrossRef]

55. Limsakul, A.; Singhruck, P. Long-term trends and variability of total and extreme precipitation in Thailand. *Atmos. Res.* **2016**, *169*, 301–317. [CrossRef]

56. Feng, L.; Zhou, T. Water vapor transport for summer precipitation over the Tibetan Plateau: Multidata set analysis. *J. Geophys. Res. Space Phys.* **2012**, *117*. [CrossRef]

57. Lehmann, E.L. *Nonparametrics: Statistical Methods Based on Ranks*; Holden-Day: Clear Spring, MD, USA, 1975.

58. Sneyers, R. *On the Statistical Analysis of Series of Observations*; Technical Note No. 143, WMO No. 415; World Meteorological Organization: Geneva, Switzerland, 1990.

59. Yao, T.; Zhou, H.; Yang, X. Indian monsoon influences altitude effect of δ18O in precipitation/river water on the Tibetan Plateau. *Sci. Bull.* **2009**, *54*, 2724–2731. [CrossRef]

60. Schiemann, R.; Lüthi, D.; Schär, C. Seasonality and Interannual Variability of the Westerly Jet in the Tibetan Plateau Region. *J. Clim.* **2009**, *22*, 2940–2957. [CrossRef]

61. Duan, X.; Tao, Y.; Mei-Ling, X.U.; Ya-Bin, L.U.; Liang, H.L. Influence of south branch trough of westerlies on weather of Yunnan province. *Plateau Meteorol.* **2012**, *31*, 1059–1065. (In Chinese)
62. Yao, T.; Thompson, L.; Yang, W.; Yu, W.; Gao, Y.; Guo, X.; Yang, X.; Duan, K.; Zhao, H.; Xu, B.; et al. Different glacier status with atmospheric circulations in Tibetan Plateau and surroundings. *Nat. Clim. Chang.* **2012**, *2*, 663–667. [CrossRef]
63. Maussion, F.; Scherer, D.; Mölg, T.; Collier, E.; Curio, J.; Finkelnburg, R. Precipitation Seasonality and Variability over the Tibetan Plateau as Resolved by the High Asia Reanalysis. *J. Clim.* **2014**, *27*, 1910–1927. [CrossRef]
64. Sun, B.; Wang, H. Interannual Variation of the Spring and Summer Precipitation over the Three River Source Region in China and the Associated Regimes. *J. Clim.* **2018**, *31*, 7441–7457. [CrossRef]
65. Zhou, T.; Gao, J.; Zhao, Y.; Zhang, L.; Zhang, W. Water Vapor Transport Processes on Asian Water Tower. *Bull. Chin. Acad. Sci.* **2019**, *34*, 1210–1219. (In Chinese) [CrossRef]
66. Lin, C.; Chen, D.; Yang, K.; Ou, T. Impact of model resolution on simulating the water vapor transport through the central Himalayas: Implication for models' wet bias over the Tibetan Plateau. *Clim. Dyn.* **2018**, *51*, 3195–3207. [CrossRef]